On the origin of the solar cycle modulation of the winter North Atlantic Oscillation

Yuhji Kuroda[1] and Hitoshi Mukougawa[2]

[1]Meteorological Research Institute
[2]Graduate School of Science, Kyoto University

November 22, 2022

Abstract

Previous studies show that the variability associated with the winter-mean North Atlantic Oscillation (NAO) tends to be largely modulated according to the solar cycle so that the anomalous zonal wind signal extends to the upper stratosphere when solar activity is high, but the vertical extension is limited when solar activity is low. To examine the physical mechanism of the solar cycle modulation of the winter-mean NAO, momentum and wave-energy budget analyses have been performed using the Japanese Reanalysis (JRA-55) dataset from 1958 to 2021. Momentum analysis shows that the enhancement of zonal wind in High Solar (HS) years is due to direct enhancement of wave forcing. Wave-energy analysis shows that baroclinic energy conversion from zonal-mean flow in the region from the surface to the middle stratosphere and barotropic energy conversion to the zonal-mean flow around the middle stratosphere tend to be enhanced in HS winters. Both enhancements are related to the enhancement of the zonal wind. Our analysis suggests that the climatological basic states tend to become more unstable during HS winters.

On the origin of the solar cycle modulation of the winter North Atlantic Oscillation

Yuhji Kuroda[1,2] and Hitoshi Mukougawa[3]

[1]Meteorological College, Kashiwa, Japan

[2]Meteorological Research Institute, Tsukuba, Japan

[3]Graduate School of Science, Kyoto University, Kyoto, Japan

Corresponding author: Yuhji Kuroda (kuroda@mri-jma.go.jp)

Key Points:

The mechanism of solar cycle modulation of winter NAO is examined through momentum and energy analyses of a reanalysis dataset

Acceleration produced by waves in winter stratosphere associated with winter NAO tends to be enhanced in high solar years

Energy conversions between eddies and zonal-mean flow associated with winter NAO correspond well with enhanced zonal wind in high solar years

Abstract

Previous studies show that the variability associated with the winter-mean North Atlantic Oscillation (NAO) tends to be largely modulated according to the solar cycle so that the anomalous zonal wind signal extends to the upper stratosphere when solar activity is high, but the vertical extension is limited when solar activity is low. To examine the physical mechanism of the solar cycle modulation of the winter-mean NAO, momentum and wave-energy budget analyses have been performed using the Japanese Reanalysis (JRA-55) dataset from 1958 to 2021. Momentum analysis shows that the enhancement of zonal wind in High Solar (HS) years is

26 due to direct enhancement of wave forcing. Wave-energy analysis shows that baroclinic energy

27 conversion from zonal-mean flow in the region from the surface to the middle stratosphere and

28 barotropic energy conversion to the zonal-mean flow around the middle stratosphere tend to be

29 enhanced in HS winters. Both enhancements are related to the enhancement of the zonal wind.

30 Our analysis suggests that the climatological basic states tend to become more unstable during

31 HS winters.

32

Plain Language Summary

34 To examine the physical source of the solar cycle modulation of the winter-mean North Atlantic

35 Oscillation (NAO), the momentum and wave-energy budget are analyzed using the 63-winter

36 record of the reanalysis dataset. These analyses show that (1) the zonal-mean momentum

37 acceleration is driven by eddies throughout the entire depth of the atmosphere around 60° N, (2)

38 the barotropic energy conversion from eddies to zonal-mean flow is centered in the middle

39 stratosphere around 55° N, and (3) the baroclinic energy conversion from zonal-mean flow to

40 eddies from the surface to the middle stratosphere around 60° N tends to be enhanced from

41 December to February associated with the positive winter-mean NAO index in High Solar (HS)

42 activity years. These energy transfers are closely related to enhanced zonal wind. These analyses

43 suggest that the structural modulation of the NAO due to the solar cycle comes from the

44 enhanced sensitivity of the wave-mean flow interaction in the stratosphere in HS years, which is

45 broadly shared with the solar cycle modulation of the late-winter Southern Annular Mode (SAM).

46

47 **1. Introduction**

48   Much evidence has been recognized in recent years regarding the influence of the 11-year

49 solar cycle on climate (e.g., Gray et al., 2010). Examples of recent solar-climate research include

50 studies on changes of the Walker circulation (Misios et al., 2019), climate change for a future

51 grand solar minimum (Chiodo et al., 2016), change of the planetary waves in the stratosphere

52 (Lu et al., 2017a, b), and changes in the North Atlantic Oscillation (NAO) (Thieblemont et al.,

53 2015; Gray et al., 2016; Kuroda et al., 2022). Because the NAO significantly affects climate in

54 North America, and Eurasia (Hurrell et al., 2003), it is a very important climate mode of

55 variability. Up to now, most studies of the NAO have focused mainly on the appearance of the

56   NAO associated with the solar cycle, such as the role of the solar cycle on the decadal NAO
57   variability (Thieblemont et al., 2015).

58   However, there are other interesting types of problems related to both the solar cycle and the
59   NAO. Structural modulation of the NAO due to the solar cycle is one such important example. In
60   this case, solar cycle change of the meteorological fields associated with the NAO index rather
61   than the climatological NAO and the other climatological fields is a problem. In fact, observation
62   shows that the zonal wind signal associated with the winter-mean NAO tends to extend to the
63   upper stratosphere (Kodera, 2002, 2003) and persists until the following summer (Ogi et al.,
64   2003) for winters of High Solar (HS) activity, but such a signal does not appear for winters of
65   Low Solar (LS) activity. Interestingly, a similar phenomenon is observed in the Southern
66   Hemisphere (SH); the zonal wind signal associated with the Southern Annular Mode (SAM)
67   during the late winter to spring tends to extend to the upper stratosphere and persist until the
68   following summer in HS years, but such a signal does not appear for LS years (Kuroda and
69   Kodera, 2005). Note that both winter in the Northern Hemisphere (NH) and late winter to spring
70   in the SH are the seasons when the dynamical interaction between the stratosphere and
71   troposphere is most active during the year. Thompson and Wallace (2000) have labeled such
72   seasons as "active seasons". Therefore, such observational evidence can be briefly summarized
73   as follows: The zonal wind signal associated with annular modes (NAO in the NH or SAM in the
74   SH) in an active season tends to extend to the upper stratosphere and have enhanced persistence
75   across seasons in years of HS activity. Thus, it is expected that some common physical
76   mechanism exists behind the phenomenon.

77   In a previous study (Kuroda, 2018; hereafter K18), momentum and energy budget analyses
78   were performed to examine the mechanism of the solar cycle modulation of the SAM. The
79   results suggested that the interaction between zonal-mean fields and waves tends to be strongly
80   influenced by solar activity so that small changes in the strength of upward propagating waves
81   tend to be enlarged in the stratosphere during years of HS activity. In other words, the sensitivity
82   of the wave-mean flow interaction tends to be strongly enhanced in the stratosphere when solar
83   activity is high. In view of the similarity between the northern and southern annular modes, it is
84   of interest to examine the case of the solar cycle modulation of the NAO.

85   In this paper we present momentum and energy budget analyses of the solar cycle

86   modulation of the winter NAO, and we compare the results with those of the solar cycle

87   modulation of the SAM.

88   The remainder of this paper is organized as follows. Section 2 describes the data and

89   principal analytical methods, Section 3 presents the results of the momentum and energy budget

90   analyses, and Section 4 provides a discussion.

91

92   **2. Methods**

93   **2.1. Data and statistical methods**

94   The data used in this study, which cover 64 years, came from the Japanese 55-year

95   reanalysis (JRA-55) dataset from January 1958 to April 2021 (Kobayashi et al., 2015) The

96   dataset is provided on a $1.25° \times 1.25°$ longitude–latitude grid with 37 vertical pressure levels

97   from 1000 to 1 hPa. The present statistical analysis is based on a monthly mean dataset. On the

98   other hand, second or higher order quantities such as eddy forcings, the terms used in the wave-

99   energy equation, and the Eliassen-Palm (E-P) flux are first calculated at six-hour intervals and

100 then averaged for each month. Similarly, evaluations of the zonal-wind acceleration produced by

101 each forcing are first calculated at daily intervals and then averaged monthly. Frictional forcing

102 and diabatic heating were evaluated as residuals of the three-dimensional momentum or

103 thermodynamic equations using the six-hour data. Note that although the residual term of the

104 zonal momentum equation is referred to as "frictional forcing" throughout this paper, it also

105 includes the effects of turbulent processes associated with Rossby wave breaking, those of

106 gravity wave drag and other parameterized processes.

107 To examine the solar influence on the winter NAO, the data were first stratified

108 according to solar activity. The December-to-February mean F10.7 index was used as a proxy for

109 the solar activity. The original monthly mean F10.7 data were obtained through Natural

110 Resources Canada. High Solar (HS) winters were defined when the mean F10.7 indices for

111 December to February were greater than 130, and Low Solar (LS) winters when the indices were

112 less than 90. The 63-winter record contains 24 HS winters and 25 LS winters.

113 The NAO was obtained as the leading month-to-month variability of the sea level

114 pressure (SLP) during extended winter (November to April) over the North Atlantic region from

115 $20°$ to $70°$ N and from $90°$ W to $40°$ E, following the definition by Hurrell et al. (2003). The

116 NAO explains 32% of the total variance, which is far larger than the second mode that explains

117 21%. The spatial pattern obtained shows a typical meridional dipole structure with a negative

118 center of –7 hPa over Iceland and positive center of 5 hPa over the Azores (not shown).

119

120 **2.2. Momentum equations**

121 The key momentum diagnosis technique used in this study is based on the zonal-mean

122 primitive equations as described in Kuroda (2016), which are given by

$$\frac{\partial \overline{u}}{\partial t} = 2\Omega \overline{v} \sin\phi + \overline{F}_e + \overline{F}_n + \overline{X},$$

$$2\Omega \overline{u} \sin\phi + \frac{1}{a}\frac{\partial \overline{\Phi}}{\partial \phi} = \overline{J},$$

$$\frac{\partial \overline{\Phi}}{\partial p} = -\frac{R\overline{T}}{p}, \tag{1}$$

$$\frac{\partial \overline{T}}{\partial t} = \Gamma \overline{\omega} + \overline{Q}_e + \overline{Q}_n + \overline{S},$$

$$\frac{1}{a\cos\phi}\frac{\partial}{\partial \phi}\left(\overline{v}\cos\phi\right) + \frac{\partial \overline{\omega}}{\partial p} = 0,$$

131 where the overbar represents zonal-mean averaging and $\overline{\omega}$ is vertical pressure velocity. Here, $\overline{F}_e$

132 ($\overline{Q}_e$) is mechanical (thermal) wave forcing defined by

$$\overline{F}_e = -\frac{1}{a\cos^2\phi}\frac{\partial}{\partial \phi}\left(\overline{u'v'}\cos^2\phi\right) - \frac{\partial}{\partial p}\left(\overline{u'\omega'}\right), \tag{2}$$

$$\overline{Q}_e = -\frac{1}{a\cos\phi}\frac{\partial}{\partial \phi}\left(\overline{T'v'}\cos\phi\right) - \frac{\partial}{\partial p}\left(\overline{T'\omega'}\right) + \frac{\kappa}{p}\overline{T'\omega'},$$

136 $\overline{F}_n$ ($\overline{Q}_n$) is nonlinear advection term, $\overline{X}$ is frictional forcing, $\overline{S}$ is diabatic heating, $\overline{J}$ represents

137 all terms that lead to a departure from the geostrophic-wind balance, and the other symbols

138 follow the usual conventions (e.g., Andrews et al., 1987).

139 From these equations, an elliptical differential equation of the vertical pressure velocity

140 $\overline{\omega}$ can be easily obtained:

$$\frac{1}{\cos\phi}\frac{\partial}{\partial\phi}\left(\frac{\cos\phi}{\sin^2\phi}\frac{\partial\bar{\omega}}{\partial\phi}\right)+\frac{4\Omega^2 a^2 p}{R\Gamma}\frac{\partial^2\bar{\omega}}{\partial p^2}$$

$$=\frac{2\Omega ap}{R\Gamma\cos\phi}\frac{\partial}{\partial\phi}\left[\frac{\cos\phi}{\sin\phi}\frac{\partial}{\partial p}(\bar{F}_e+\bar{F}_n+\bar{X}-\frac{\dot{\bar{J}}}{2\Omega\sin\phi})\right] \qquad (3)$$

$$-\frac{1}{\Gamma\cos\phi}\frac{\partial}{\partial\phi}\left[\frac{\cos\phi}{\sin^2\phi}\frac{\partial}{\partial\phi}(\bar{Q}_e+\bar{Q}_n+\bar{S})\right],$$

142 where the dot represents the time derivative. The boundary conditions should be an approximate

143 form of $\overline{D\Phi/Dt}=0$ at the 1000 hPa level, $\bar{\omega}=0$ for the uppermost level, and $\bar{v}=0$ at

144 $\phi=\pm\pi/2$.

145   The solution of equation (3) with boundary conditions can be represented symbolically

146 as

$$\bar{\omega}=(\mathbf{L}-\mathbf{A}_1\mathbf{B}-\mathbf{A}_3\mathbf{C})^{-1}[\mathbf{A}_1(\bar{F}_e+\bar{X})+\mathbf{A}_2\dot{\bar{J}}+\mathbf{A}_3(\bar{Q}_e+\bar{S})], \qquad (4)$$

148 because the nonlinear advection terms $\bar{F}_n$ and $\bar{Q}_n$ in equation (3) can be represented by

149 $\bar{F}_n=\mathbf{B}\bar{\omega}$, $\bar{Q}_n=\mathbf{C}\bar{\omega}$. Here $\mathbf{L}$, $\mathbf{A}_i$ ($i=1,2,3$), $\mathbf{B}$, and $\mathbf{C}$ are linear operators representing

150 differential or differential-integral operators (Kuroda, 2016). Similarly, from equation (1a) the

151 zonal-mean zonal wind acceleration can also be represented as

$$\frac{\partial\bar{u}}{\partial t}=\{(2\Omega\sin\phi\mathbf{M}+\mathbf{B})(\mathbf{L}-\mathbf{A}_1\mathbf{B}-\mathbf{A}_3\mathbf{C})^{-1}\mathbf{A}_1+\mathbf{I}\}(\bar{F}_e+\bar{X})$$

$$\qquad (5)$$

$$+\{(2\Omega\sin\phi\mathbf{M}+\mathbf{B})(\mathbf{L}-\mathbf{A}_1\mathbf{B}-\mathbf{A}_3\mathbf{C})^{-1}\}[\mathbf{A}_2\dot{\bar{J}}+\mathbf{A}_3(\bar{Q}_e+\bar{S})],$$

153 where $\mathbf{I}$ and $\mathbf{M}$ are the identity and a linear differential-integral operators, respectively. Because

154 equation (5) is also linear with respect to the forcings, the acceleration produced by each forcing

155 can be evaluated separately. Thus, the component of acceleration produced by all eddies alone,

156 for example, can be evaluated by

$$\left(\frac{\partial\bar{u}}{\partial t}\right)_e=\{(2\Omega\sin\phi\mathbf{M}+\mathbf{B})(\mathbf{L}-\mathbf{A}_1\mathbf{B}-\mathbf{A}_3\mathbf{C})^{-1}\mathbf{A}_1+\mathbf{I}\}\bar{F}_e$$

$$\qquad (6)$$

$$+\{(2\Omega\sin\phi\mathbf{M}+\mathbf{B})(\mathbf{L}-\mathbf{A}_1\mathbf{B}-\mathbf{A}_3\mathbf{C})^{-1}\}\mathbf{A}_3\bar{Q}_e.$$

158   Note that the right-hand side of the equation can be uniquely determined by eddy forcings $\bar{F}_e$

159   and $\bar{Q}_e$ of all waves, but is not directly affected by other types of forcing such as diabatic heating

160   or friction. In such a way, the component of acceleration due to each forcing can be evaluated.

161   The diagnostic model used in this study is essentially the same, except that it uses the

162   log-pressure coordinate for the vertical coordinate as in K18 (see Appendix A of K18). The

163   present model used 101 vertical layers with a vertical resolution of 600 m. This placed the top of

164   the model substantially above the top of the original data (1 hPa) so that the rigid upper boundary

165   condition of $\bar{w} = 0$ would not affect the diagnosis. The same input data as were used for the 1-

166   hPa level were used for all levels above 1 hPa. Other important settings were as follows: For the

167   meridional direction, 501 cells were used at equal intervals of the sine of the latitude with 500

168   Hough modes for the formulation by Kuroda (2016); higher meridional resolution was used to

169   have better accuracy in the high-latitude region; and the diagnosis was performed daily using

170   daily-mean forcings because preliminary calculations showed that the results were almost the

171   same as those using 6-hourly calculations.

172

173   **2.3. Wave-energy equation**

174   The wave-energy equation representing energy transfer between atmospheric waves and

175   other external fields, including the zonal-mean fields used in the present study, is given by

176   Holton (1975). Its integral form is

177    $$\frac{d}{dt}(K'+P') + W = \{\bar{K}, K'\} + \{\bar{P}, P'\} + D, \tag{7}$$

178   where K' and $\bar{K}$ are the kinetic energies of the eddies and zonal-mean fields, respectively; P'
179   and $\bar{P}$ are the available potential energies of the eddies and zonal-mean fields, respectively; W
180   is the surface integral of the wave-energy flux; $\{\bar{K}, K'\}$ is the energy conversion from $\bar{K}$ to K'
181   (barotropic energy conversion); $\{\bar{P}, P'\}$ is the energy conversion from $\bar{P}$ to P' (baroclinic
182   energy conversion); and D is the sum of the external forcings and dissipation terms. The
183   integrands $\varepsilon(\bar{K}, K')$ and $\varepsilon(\bar{P}, P')$ of $\{\bar{K}, K'\}$ and $\{\bar{P}, P'\}$ (e.g., $\{\bar{K}, K'\} \equiv \int d^3 x \varepsilon(\bar{K}, K')$) are
184   written as

185    $$\begin{aligned}\varepsilon(\bar{K}, K') = -\rho_0 (\overline{u'v'}\frac{1}{a}\frac{\partial \bar{u}}{\partial \phi} + \overline{u'w'}\frac{\partial \bar{u}}{\partial z} + \overline{v'^2}\frac{1}{a}\frac{\partial \bar{v}}{\partial \phi} \\ + \overline{v'w'}\frac{\partial \bar{v}}{\partial z} + \bar{u}\overline{u'v'}\frac{\tan \phi}{a} - \bar{v}\overline{u'^2}\frac{\tan \phi}{a}),\end{aligned} \tag{8}$$

186   and

$$\varepsilon(\bar{P}, P') = -\rho_0 \frac{R^2}{N^2 H^2} (\overline{v'T'} \frac{1}{a} \frac{\partial \bar{T}}{\partial \phi} + \overline{w'T'} \frac{\partial \bar{T}}{\partial z}). \qquad (9)$$

188   Here, all the terms are represented by the log-pressure coordinate, and $\rho_0(z), R, H$, and N^2 are
189   the basic density, the gas constant for dry air, the mean scale height, and the square of the
190   buoyancy frequency, respectively (see Andrews et al., 1987).
191   The integrand $\varepsilon(D)$ of D is written as

$$\varepsilon(D) = \rho_0 (\overline{u'X'} + \overline{v'Y'}) + \frac{R^2 \rho_0}{H^2 N^2} \overline{S'T'}, \qquad (10)$$

193   where X', Y', and S' are the eddy components of the zonal and meridional frictions, and

194   diabatic heating, respectively.

195   This study used the space–time form of equation (7) to evaluate the spatial distribution of

196   energy transfers from the zonal-mean flow to eddies. Energy diagnoses were performed using the

197   six-hourly reanalysis dataset, and the barotropic energy conversion rate, for example, was

198   evaluated from equation (8).

199

200   **2.4. Regressions**

201   Figures 2 to 9 show regressions against the December-to-February mean NAO index,

202   which were calculated separately for 24 HS and 25 LS years. Namely, if zonal wind and the

203   December-to-February mean NAO index of i-th HS years are denoted by $U_{HS(i)}$ and $a_{HS(i)}$,

204   respectively, then the regression of the zonal wind for HS years is calculated by $<U_{HS(i)} a_{HS(i)}>$,

205   where the brackets indicate time averaging of all HS years and $a_{HS(i)}$ is assumed to be

206   standardized (i.e., $<(a_{HS(i)})^2> = 1$). Regressions for other variables and for LS years are

207   similarly calculated. Note that these regressed figures correspond to a *positive* phase of the

208   December-to-February mean NAO index characterized by meridional dipole structures of

209   anomalous zonal winds in the troposphere with positive (negative) winds around 55°N (35°N)

210   from December to February. Thus, if we consider the typical cases with a negative phase of the

211   NAO index, polarities of all the signals in the regressions should be reversed.

212

213   **3. Results**

214   **3.1. Climatology**

Figure 1 compares two climatological features of zonal-mean zonal wind and temperature between HS and LS winters. Although December to February is the season of boreal mid-winter, the monthly peak values of the zonal wind at 1-hPa level appear in December, and the peak wind decreases with seasonal evolution (Figure 1a–e). At the same time, the polar cap temperature in the lower stratosphere has the lowest value in December, and it increases with seasonal evolution (Figure 1k–o).
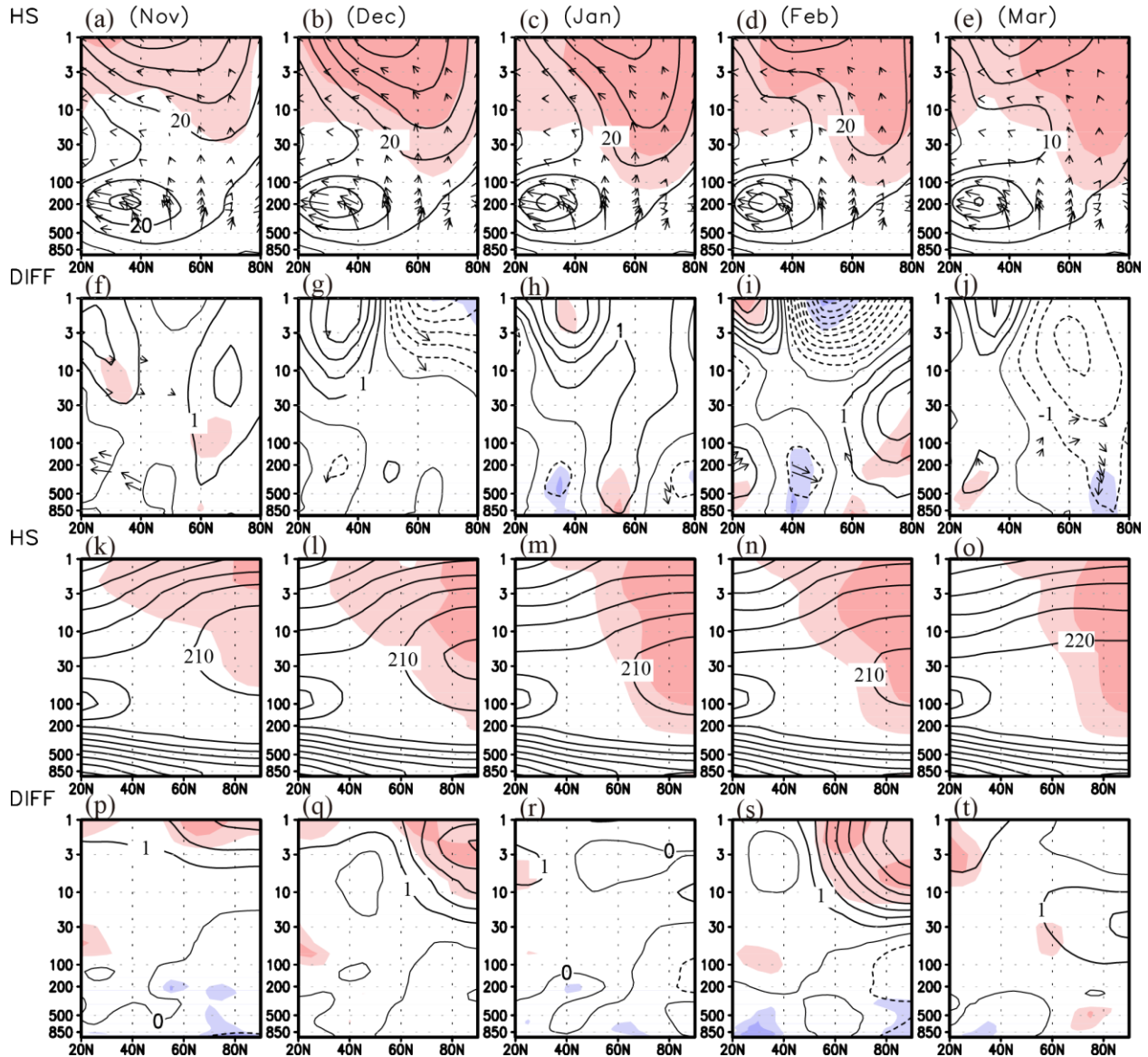

Figure 1. Height–latitude plots of climatological (1958–2021) conditions for November to March. (a–e) Monthly zonal-mean zonal wind (contours) and E-P flux (arrows) for HS winters. Contour interval is 10 m s^{-1}; dashed contours have negative values. Light and heavy shadings indicate regions where the standard deviation of interannual zonal wind variations is greater than 5 and 10 m s^{-1}, respectively; pink is positive and blue is negative. (f–j) Difference in zonal wind (contours) and E-P flux (arrows) between HS and LS winters (HS-LS). Contour interval is 1 m s^{-}

1. Shadings indicate regions where the statistical significance greater than 95% by Student's *t*-test, and pink (blue) colored regions are where the difference is positive (negative). Arrows in (a–j) are scaled by the reciprocal square root of pressure; (f–j) show only arrows that are statistically significant at 95%. (k–o) Monthly zonal-mean temperature (contours) for HS winters. Contour interval is 10 K. Light and heavy shadings indicate regions where the standard deviation of interannual zonal-mean temperature variations is greater than 3 K and 6 K. (p–t) Difference in zonal-mean temperature between HS and LS winters. Contour interval is 1 K. Light (heavy) shadings indicate that the statistical significance is greater than 95 (99) % by Student's *t*-test.

Regarding the difference in zonal winds between HS and LS winters, although the statistical significance is weak, a meridional dipole structure in the middle to upper stratosphere with an anomalous westerly in the subtropics persists throughout the winter, except for November when another westerly anomaly exists in the middle stratosphere of the polar area (Figure 1f–j). Another one is that associated with the Polar-night Jet Oscillation (PJO), showing poleward and downward movement of the anomalous zonal wind. Although the statistical significance is very weak and upward extension of the westerly signal around 60° N on January is rather limited compared with a previous study (Kuroda and Kodera, 2002; Kuroda et al., 2022), traces of such a signal can be observed.

Although the anomalous positive signal of the temperature signal during HS winters in the upper stratosphere and its statistical significance are very weak compared with the previous study (Kuroda and Kodera, 2002; Kuroda et al., 2022), it is certainly exits, especially in the middle to high latitudes, except for March (Figure 1p–t). An absent or small temperature signal in the upper stratosphere associated with the solar cycle is consistent with previous studies (e.g., Kuchar et al., 2015).

3.2. Solar influence on the NAO

Figure 2 shows regression maps of the zonal-mean zonal wind and the E-P flux against the December-to-February mean NAO index calculated separately for HS and LS winters. In the troposphere, meridional dipole structures with an anomalous westerly (easterly) at high- (low-) latitude with equatorward E-P flux from December to February are commonly observed for both HS and LS winters. However, signals in the stratosphere are very different between them. In fact, a significant zonal wind signal extends to the upper stratosphere in December and gradually propagates downward as the season progresses and the peak exists around 50-hPa level on February for HS winters, but a weaker significant signal extends only up to the lower

stratosphere, and downward propagation is unclear for LS winters. Monte Carlo simulations of the 24- and 25-year samples with 10,000 random shuffles show that there is only a 6.2% probability that the 95% significance region from December to January in Figure 2 could appears more by chance (i.e., the present signal is statistically significant at the 93% level). Excluding years with large volcanic eruptions or small changes of the threshold values in the definitions of HS and LS years do not change the results significantly. At the same time, the corresponding sea level pressure (SLP) signal tends to show more annular structure for HS winters, but is more locally restricted in the north Atlantic for LS winters (not shown). Such characteristics of the solar cycle modulation of the winter NAO are very similar to those obtained in a previous study (Kodera, 2002).
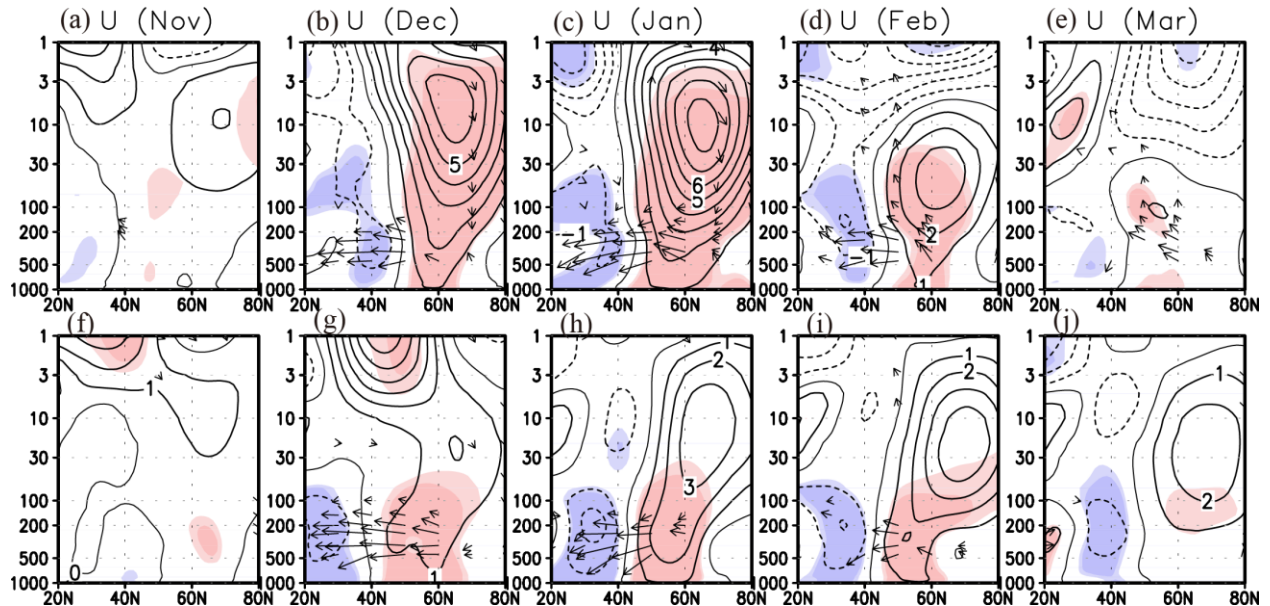
Figure 2. Regressions of zonal-mean zonal wind (contours) and E-P flux (arrows) anomalies against the December-February mean NAO index for (a–e) HS and (f–j) LS winters. Contour interval is 1 m s^{-1}, and dashed contours indicate negative values. Light (heavy) shading indicates areas of statistical significance at the 90 (95) % confidence level (Student's t-test). Arrows indicate 95% statistically significant E-P flux anomalies and are scaled by the reciprocal square root of pressure.

To examine temperature changes associated with the variation of zonal wind and E-P flux, regressions of the zonal-mean temperature were also calculated (Figure 3). It can be seen that significantly large temperature signals tend to appear all winter in the upper stratosphere and over areas poleward of about 60°N for HS winters. The existence of significant positive signal from the surface at 50°N to the tropical upper troposphere is also noted. In fact, a meridional

dipole structure with a negative (positive) signal at about 40 (90) °N exists around 1 hPa, and a vertical dipole structure with a negative (positive) signal appears around 50 (1) hPa at the polar cap in January. In contrast, the temperature signal in LS winters tends to be very weak and is not so prominent, especially in the stratosphere. Thus, the solar cycle modulation of the winter NAO is also evident in temperature fields.
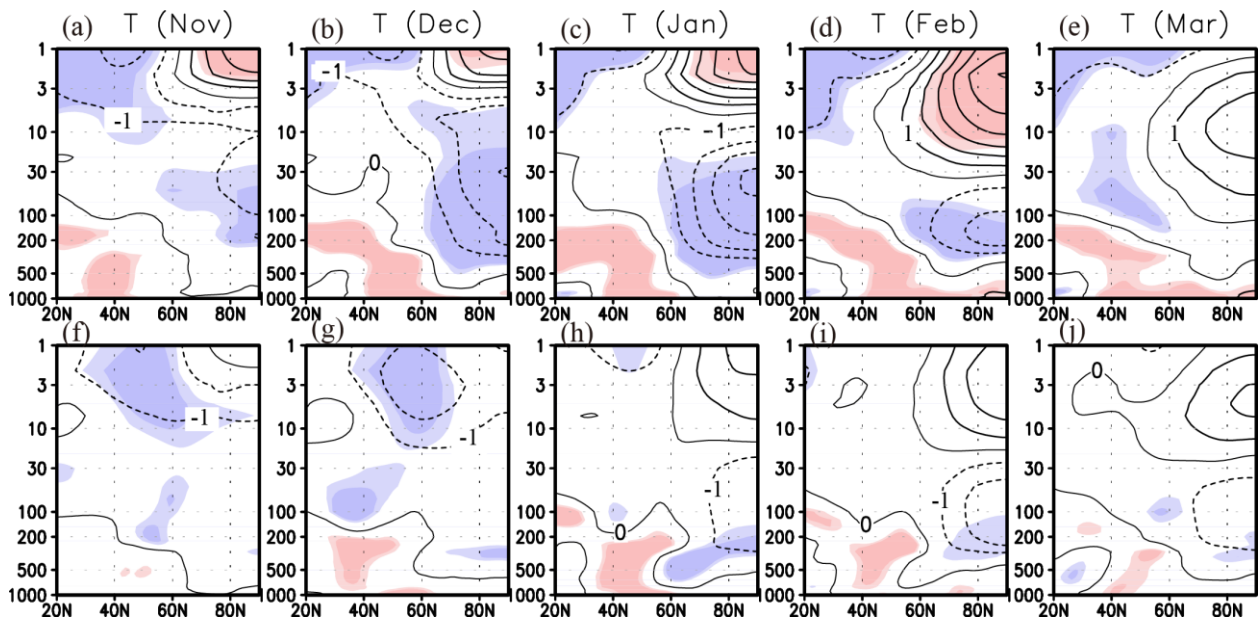

Figure 3. Regressions of zonal-mean temperature (contours) against the December-February mean NAO index for (a–e) HS and (f–j) LS winters. Contour interval is 1 K and dashed contours indicate negative values. Light (heavy) shading indicates areas of statistical significance at the 90 (95) % confidence level (Student's *t*-test).

As the basic dynamics controls the acceleration of the zonal wind rather than the wind speed itself, the regressions of zonal wind acceleration are compared for HS and LS winters (Figure 4). It can be seen that prominent deep acceleration of zonal wind is produced in November for HS winters. In contrast, the acceleration in November is much weaker and not significant, and significant acceleration appears only in the high-latitude troposphere in December for LS winters.
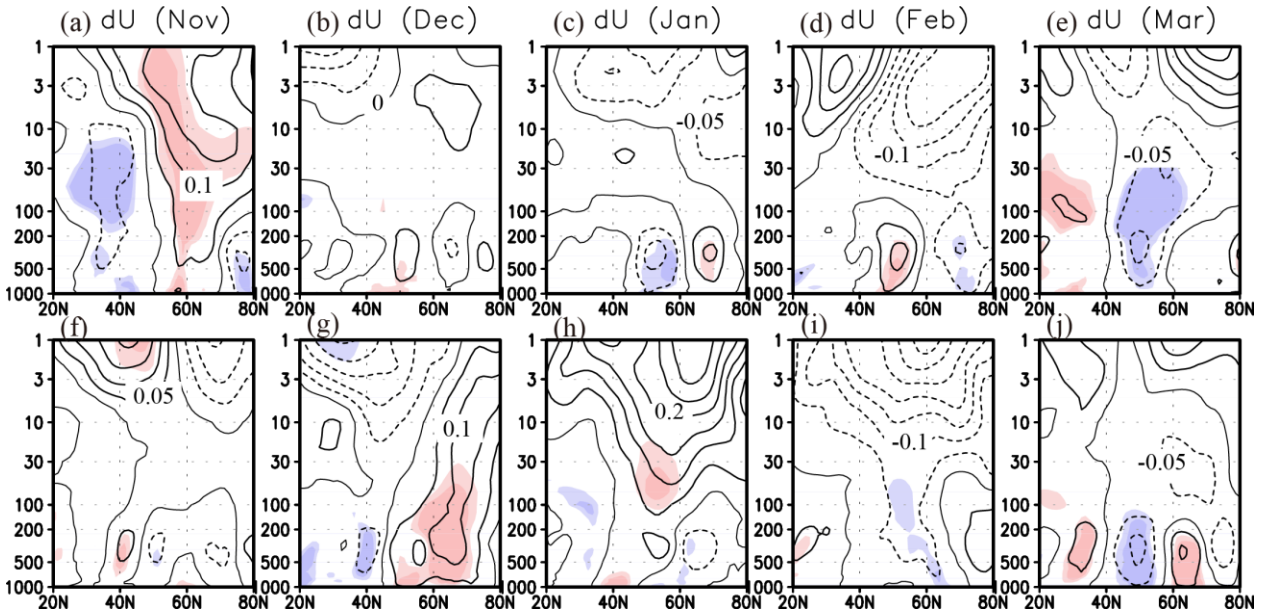
Figure 4. Regressions of the zonal-mean zonal wind acceleration against the December–February mean NAO index for (a–e) HS and (f–j) LS winters. Contour interval is 0.05 m s^{-1} d^{-1}, and dashed contours indicate negative values. Light (heavy) shadings indicate areas of statistical significance at the 90 (95) % confidence level (Student's *t*-test).

To examine how the acceleration of zonal wind is produced by eddies, Figure 5 compares the regressions of the acceleration produced by waves alone using the diagnosis equation (6). It can be seen that the area of acceleration around 60 °N extends from the surface to the upper stratosphere for December and January and to the middle stratosphere in February for HS winters, but the acceleration extends only up to the middle stratosphere for December and January and is very weak in February for LS winters. Such accelerations tend to be well offset with the acceleration produced by frictional forcings (not shown). However, as the frictional forcing tends to work passively against the zonal wind, the acceleration produced by wave forcing can be considered as a key driver producing the actual zonal wind anomaly seen in Figure 2.
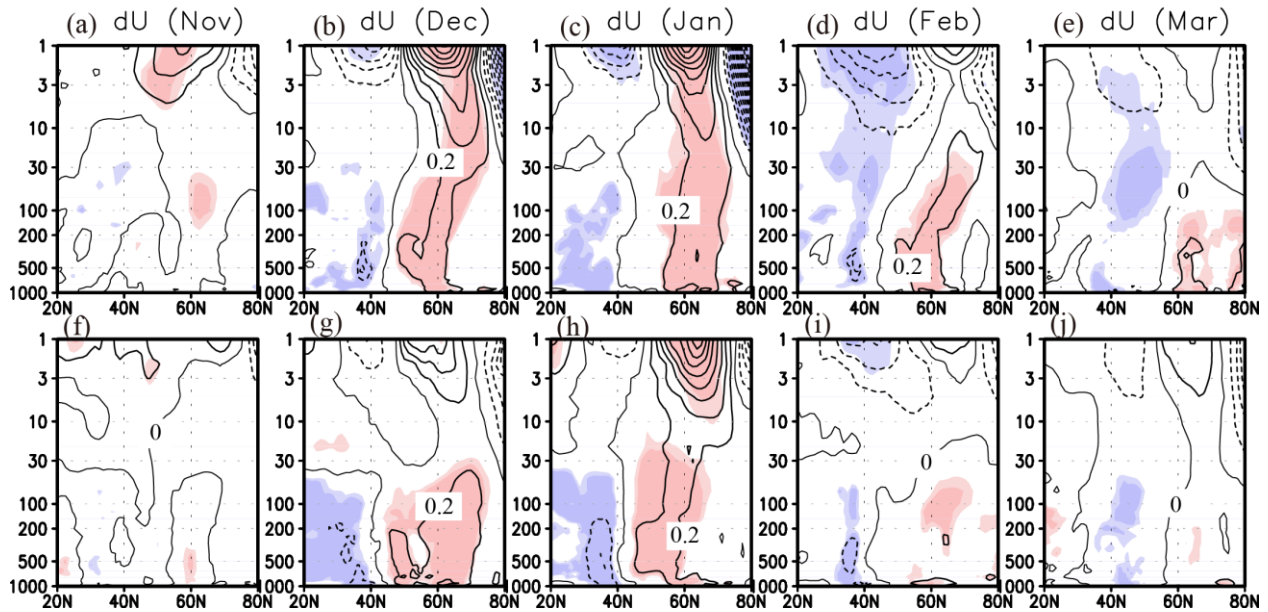
Figure 5. Regressions of the zonal-mean zonal wind acceleration produced by waves alone against the December–February mean NAO index for (a–e) HS and (f–j) LS winters. Contour interval is 0.2 m s^{-1} d^{-1}, and dashed contours indicate negative values. Light (heavy) shadings indicate areas of statistical significance at the 90 (95) % confidence level (Student's *t*-test).

Previous studies (e.g., Andrews et al., 1987; K18) showed that the zonal-wind acceleration patterns produced by waves tend to be similar to those associated with divergence of the E-P flux in the stratosphere. Note that the divergence of the E-P flux is the only wave forcing in the transformed Eulerian mean formulation (e.g., Andrews et al., 1987). The E-P fluxes and their divergences for both solar years are shown in Figure 6.

Although overall patterns of the E-P flux divergence are not very similar to those of the acceleration by eddies (Figure 5), a weak correspondence is recognized in which the acceleration regions tend to correspond to the positive regions of E-P flux divergence. For example, the anomalous divergence of the E-P flux extends from 50 to 1 hPa for December and from 100 to 1 hPa for January in HS winters, while deep divergence from 50 to 1 hPa can be observed in January for LS winters, although the statistical significances is much weaker. It is conceivable that the divergence anomaly of the E-P flux could correspond to the generation of waves in this region. It should be noted that the contour interval for the divergence of the E-P flux in Figure 6 is five times larger than that of the acceleration in the stratosphere shown in Figure 5.

These results show that the extension of anomalous westerly wind to the upper stratosphere in HS winters comes from enhancement of zonal wind acceleration produced by wave forcings from December to February. Enhanced acceleration of zonal winds by waves in

379   HS winters is common with the solar cycle modulation of the SAM (K18). However, during

380   months of enhanced wave forcings, zonal wind anomalies are very different. In fact, for the solar

381   cycle modulation of the SAM, wave-induced acceleration intensifies in August and September,

382   and is small from October to December when zonal wind anomalies are observed (K18). This is

383   because frictional effects in the stratosphere in the SH are much smaller. Hence, zonal wind

384   anomalies created in late winter tend to persist until the end of spring. In contrast, frictional

385   effects in the stratosphere during winter NH are much larger and continuous acceleration during
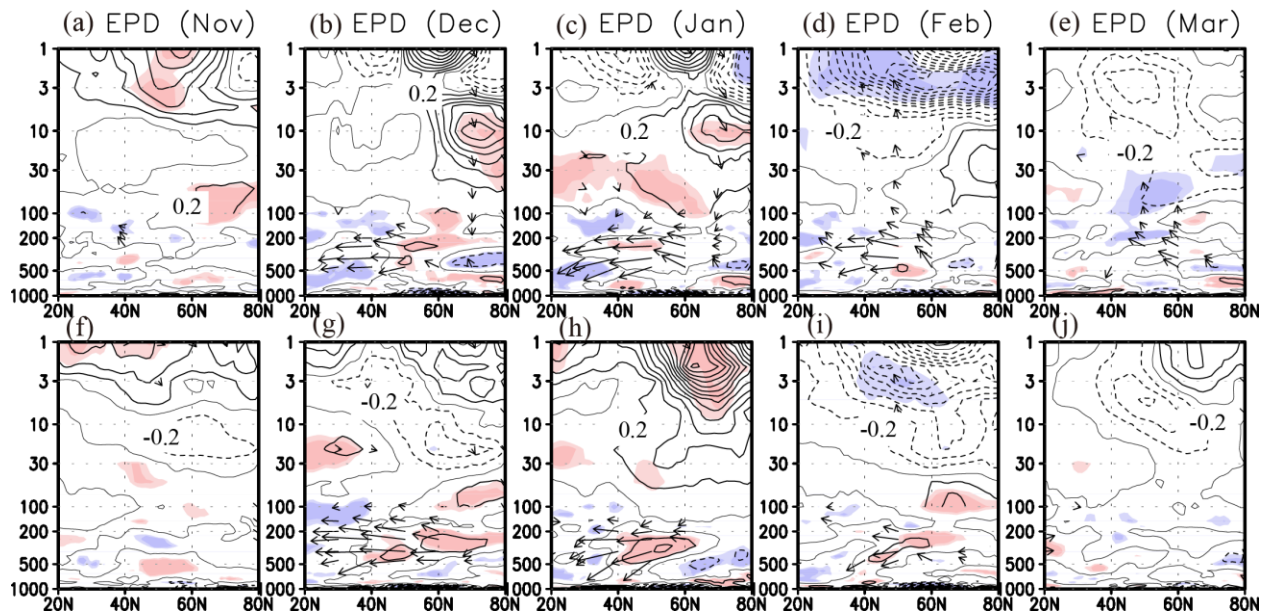
386   midwinter is needed to create zonal wind anomalies.

387

388   **Figure 6.** Regressions of the divergence (contours) of the E-P flux (arrows) against the
389   December–February mean NAO index for (a–e) HS and (f–j) LS winters. Contour intervals are
390   1.0 m s^{-1} d^{-1} up to 100 hPa and 0.2 m s^{-1} d^{-1} from 100 to 1 hPa; dashed contours indicate
391   negative values. Arrows are scaled by the reciprocal square root of pressure and are statistically
392   significant at 95%. Light (heavy) shading indicates areas of statistical significance at the 90
393   (95) % confidence level (Student's t-test).

394

395   Next, to examine how waves and zonal-mean fields interact, wave-energy budget

396   analyses were performed separately for HS and LS winters. Here the regressions of each term in

397   the right-hand side of equation (7) are compared. First, the barotropic energy conversion terms

398   (equation (8)) are compared (Figure 7). It can be seen that a significant negative signal appears in

399   the middle stratosphere in November, and it gradually shifts downward as the seasonal evolution

400   for HS winters. This signal corresponds well with anomalous westerly wind (Figure 2) and

represents the anomalous flow of kinetic energy from waves to zonal-mean winds, corresponding

to the acceleration of zonal winds. This is more clearly understood if we note that the term

$-\{\bar{K}, K'\}$ serves as a source term for the kinetic energy of the zonal-mean field (Holton, 1975).

Such negative signals from December to February also exist in the stratosphere of LS winters,

but they are weak and not significant. Thus, the present analysis of the barotropic energy

conversion is very consistent with those obtained in Figures 2 and 5.
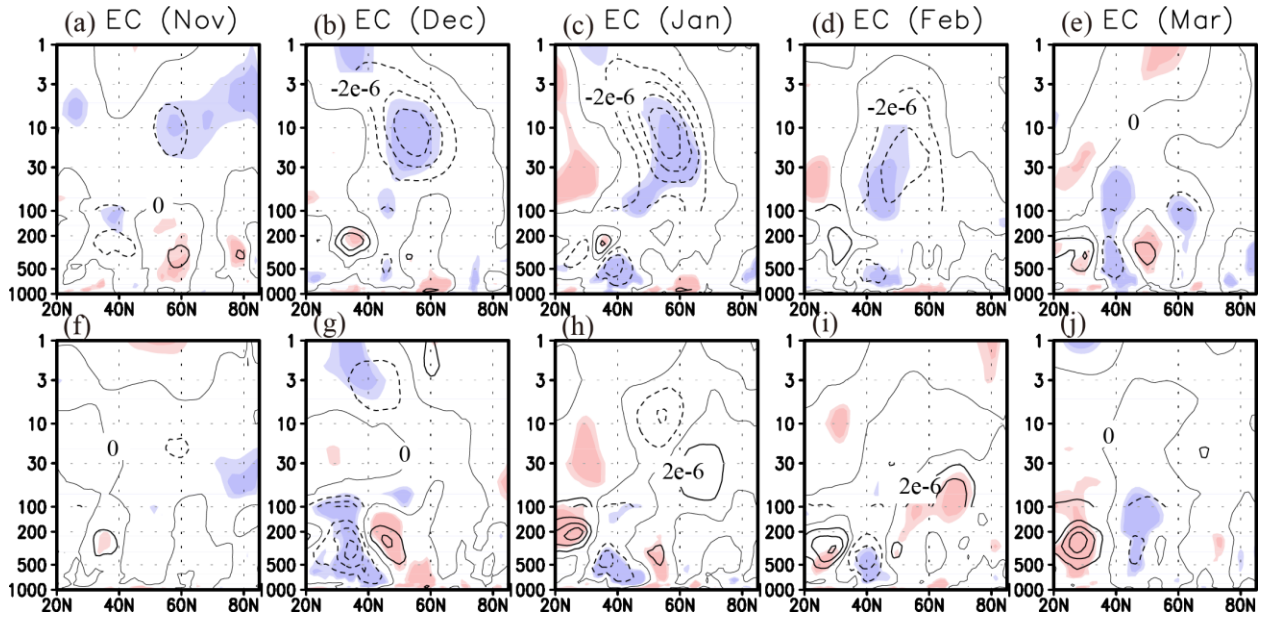
Figure 7. Regressions of barotropic energy conversion densities from zonal-mean fields against the December–February mean NAO index for (a–e) HS and (f–j) LS winters. Contour intervals are 2×10^{-5} Wm^{-3} from 1000 to 100 hPa and 2×10^{-6} Wm^{-3} from 100 to 1 hPa; dashed contours indicate negative values. Light (heavy) shading indicates areas of statistical significance at the 90 (95) % confidence level (Student's t-test).

Next, the baroclinic energy conversion terms (equation (9)) are compared (Figure 8). It

can be seen that an area of large positive energy conversion extends from the surface to the low-

latitude upper stratosphere in December and January and to the middle stratosphere for February

for HS winters, although there are only limited areas with statistical significance within the lower

stratosphere. However, although a similar weaker signal can be observed in December, it is

nearly absent or very weak in January and February for LS winters. To understand how these

signals relate to the modulation of the zonal wind, we should note that baroclinic energy

conversion tends to be more enhanced in areas of stronger vertical wind shear (e.g., Eady, 1949).

In fact, visual inspection shows that stronger vertical zonal wind shear tends to correspond with

stronger baroclinic energy conversion. For example, stronger energy conversion around 60° N in January corresponds well with stronger vertical wind shear at that latitude (Figure 2). It should also be noted that the energy conversion rate tends to be smaller with increasing altitude due to decreasing air density. Thus, enhanced baroclinic energy conversion in HS years can be regarded as the direct result of the enhanced zonal wind in those years. Although the baroclinic process tends to weaken the vertical shear of the zonal wind, the planetary waves generated there can work to accelerate the zonal wind by barotropic processes after propagating into the stratosphere, and these processes will act as positive feedback to sustain the wind strength during midwinter in HS years (Figure 7).

Note that enhanced baroclinic energy conversion in the stratosphere for HS winters compared with LS winters is also observed for the solar cycle modulation of the SAM (K18). Therefore, these results suggest that baroclinic processes tend to act as key processes in the solar cycle modulation of the annular mode.
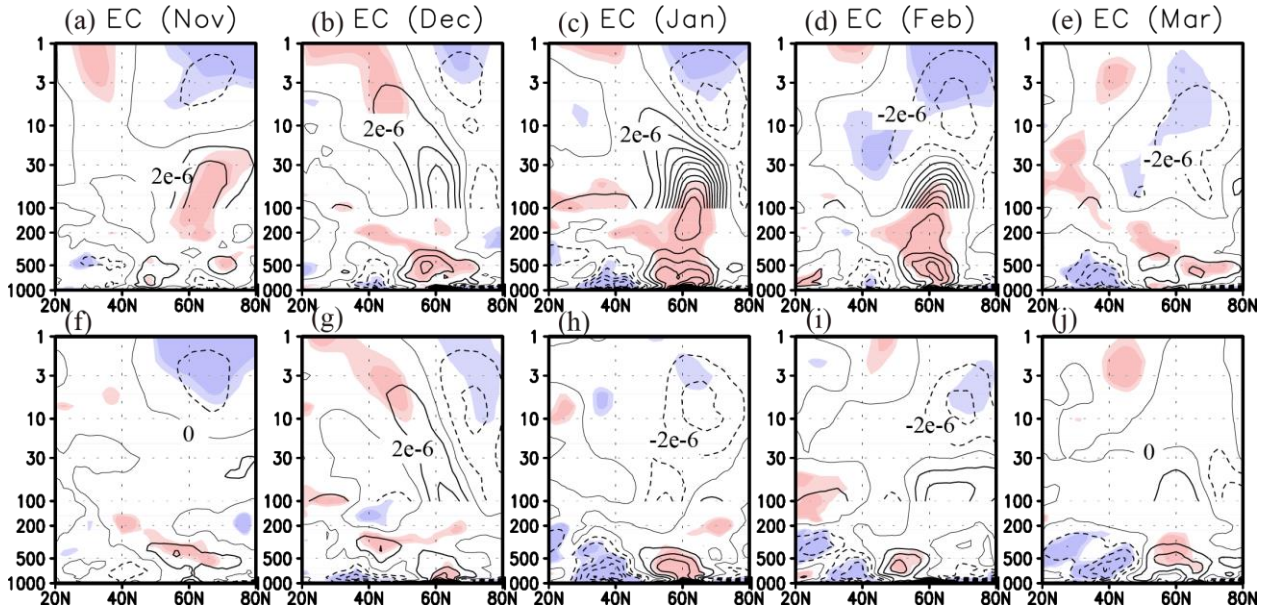

Figure 8. Regressions of baroclinic energy conversion densities from zonal-mean fields to eddies against the December–February mean NAO index for (a–e) HS and (f–j) LS winters. Contour intervals are 2×10^{-5} Wm^{-3} from 1000 to 100 hPa and 2×10^{-6} Wm^{-3} from 100 to 1 hPa; dashed contours indicate negative values. Light (heavy) shadings indicate areas of statistical significance at the 90 (95) % confidence level (Student's *t*-test).

We also compare the generation or dissipation of wave energy due to diabatic heating (equation (10)) in Figure 9. A small positive significant signal in the polar lower stratosphere in December and January can be observed in HS winters. On the other hand, there is a pronounced

positive signal at the bottom of the high-latitude troposphere. This is because when the NAO is positive, temperatures in the Arctic are cooler and heating by the oceans is enhanced. Thus, the contribution by diabatic processes is relatively minor compared with energy conversion from zonal-mean flow, although a small positive contribution at the lower stratospheric polar region in HS winters can also be noticeable.

In fact, by comparing the magnitude of diabatic processes with that of conversion processes in the case of solar cycle modulation of the SAM (K18), it is found that the contribution by diabatic processes to the winter NAO is much smaller. This may reflect the season of the solar cycle modulation of the NAO, which takes place in mid-winter, when solar heating is nearly absent around the polar cap. In contrast, solar cycle modulation of the SAM takes place from late winter to spring, when solar radiative heating begins to extend to high latitudes.
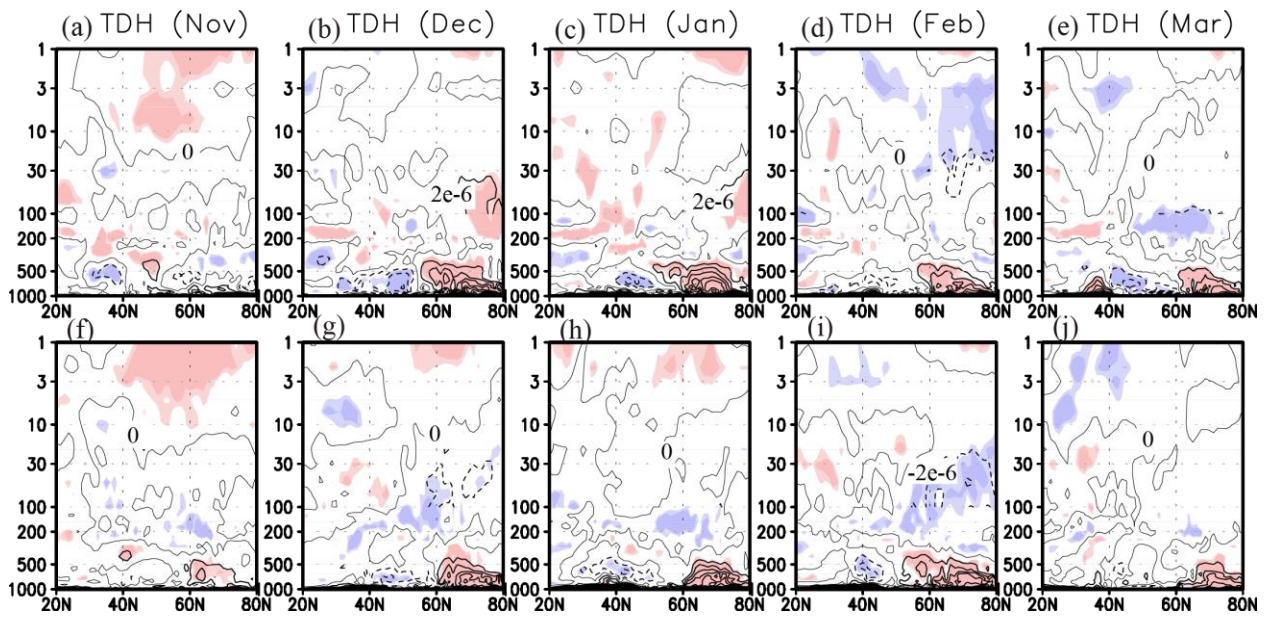

Figure 9. Regressions of input of wave energy densities from diabatic heating against the December–February mean NAO index for (a–e) HS and (f–j) LS winters. Contour intervals are 2 × 10^{-5} Wm^{-3} from 1000 to 100 hPa and 2 × 10^{-6} Wm^{-3} from 100 to 1 hPa; dashed contours indicate negative values. Light (heavy) shadings indicate areas of statistical significance at the 90 (95) % confidence level (Student's t-test).

4. Discussion

This study used momentum and energy budget analyses of the JRA-55 reanalysis dataset from 1958 to 2021 to examine physical mechanism of the solar cycle modulation of the winter

510 NAO, in comparison with the solar cycle modulation of the SAM (K18). The momentum

511 analysis showed that the solar cycle modulates the zonal wind through enhanced wave forcing

512 during the midwinter season. The wave-energy budget analysis showed that solar activity

513 enhances energy conversions (especially baroclinic conversion) between zonal-mean fields and

514 waves, whereas wave energy generation due to diabatic heating plays a secondary role.

515   In the present study, JRA-55 reanalysis data were used rather than the ERA-Interim data

516 (Dee et al., 2011) used in a previous study (K18). This is because the ERA-Interim dataset

517 includes data only after 1979, whereas JRA-55 includes data beginning from 1958, which allows

518 analysis over a longer period. Moreover, data from 1958 for the NH are considered reliable due

519 to the existence of many historical observations. However, it should also be noted that the data

520 above about 10 hPa up to 1978 were generated by data assimilation and not by direct observation

521 (e.g., Noguchi and Kobayashi, 2018). Note also that effects of solar activity such as UV change

522 have not been taken into account for the entire period when generating the reanalysis data. Thus,

523 special attention is needed for the top layer of data.

524   It should be noted that solar cycle modulation of the NAO can also be observed in more

525 recent ERA-Interim data, although it is less statistically significant. To confirm this fact, the

526 analysis was repeated using ERA-Interim data from 1979 to 2019, when remote sensing

527 observations by satellite were utilized to generate the dataset. Based on the same criteria for HS

528 and LS winters, 16 HS and 15 LS winters were identified. Regression analysis against the NAO

529 index is shown in Figure 10. As can be seen, the solar cycle modulation of the NAO is nearly the

530 same as was obtained in the present study. Momentum and energy analyses show results similar

531 to those obtained in the present study, although some results are not so clear.
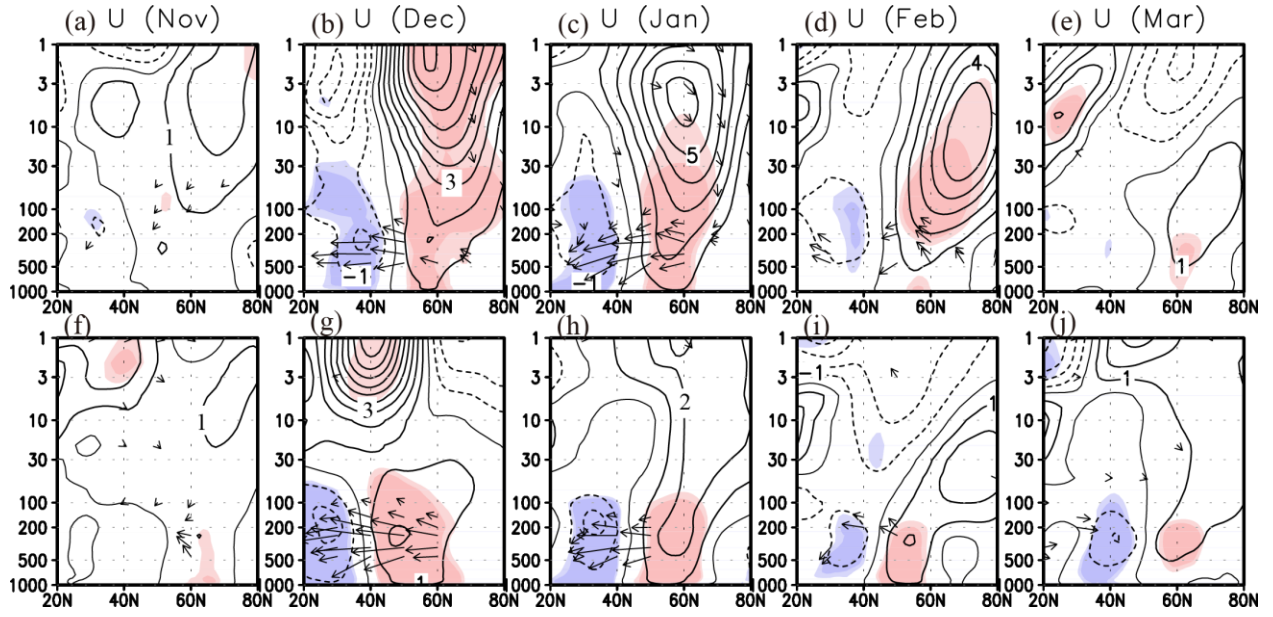
532

533
534
535
536
537
538
539
540
541
542
543
544

Figure 10. Regressions of zonal-mean zonal wind (contours) and E-P flux (arrows) against the December–February mean NAO index for (a–e) HS and (f–j) LS winters using ERA-Interim data from 1979 to 2019. Contour interval is 1 m s^{-1} and dashed contours indicate negative values. Light (heavy) shadings indicate areas of statistical significance at the 90 (95) % confidence level (Student's t-test). Arrows indicate 95% statistically significant E-P flux and are scaled by the reciprocal square root of pressure.

If the integrand of $\{\overline{K}, K'\}$ is denoted by $\varepsilon(\overline{K}, K')$, the following approximation holds from equation (8) if only the major term is kept: $\varepsilon(\overline{K}, K') \approx F_y \cdot \overline{U}_y$, where $F_y \approx -\rho_0 \overline{u'v'}$ and $\overline{U}_y$ are the meridional component of the E-P flux and the meridional gradient of the zonal-mean zonal wind, respectively. Thus, the anomaly will satisfy $\delta\varepsilon(\overline{K}, K') \approx \delta F_y \cdot (\overline{U}_y)_c + (F_y)_c \cdot \delta\overline{U}_y$, where $(*)_c$ and $\delta(*)$ represent climatological and anomalous quantities, respectively. If we note that $(\overline{U}_y)_c$ is positive (negative) for the equatorial (polar) side of the jet, the first term becomes negative if δF_y is negative (positive) for the equatorial (polar) side of the jet. This means that the meridionally E-P flux is divergent around the jet axis and consistent with the condition of wave-acceleration in HS winters (Figure 7). Similarly, because $(F_y)_c$ is negative throughout the winter (Figure 1), the second term will also be negative if $\delta\overline{U}_y$ is positive; the equatorial side of the anomalous wind satisfies this condition in HS winters. Thus, negative barotropic conversion at the stratosphere in HS winters is consistent with enhanced anomalous zonal wind in the stratosphere. Therefore, this process further accelerates the zonal winds when positive zonal wind anomalies are formed in HS winters.

580   A similar discussion is possible for the process of baroclinic energy conversion. In fact,

581   we can obtain the approximate relation $\varepsilon(\overline{P}, P') \approx F_z \cdot \overline{U}_z$ if only the major term is kept in

582   equation (9) and the thermal wind relationship is used. Here the integrand of $\{\overline{P}, P'\}$ is denoted

583   by $\varepsilon(\overline{P}, P')$, $F_z \approx \rho_0 f_0 R \overline{v'T'}/HN^2$ and $\overline{U}_z$ are the vertical component of the E-P flux and the

584   vertical gradient of the zonal-mean zonal wind, respectively. If we use the relation

585     $\delta\varepsilon(\overline{P}, P') \approx \delta F_z \cdot (\overline{U}_z)_c + (F_z)_c \cdot \delta\overline{U}_z$ and note that both $(\overline{U}_z)_c$ and $(F_z)_c$ tend to be positive

586   (Figure 1), the sign of the first term is determined by that of δF_z, whereas the sign of the second

587   term is determined by that of $\delta\overline{U}_z$. From Figure 2, we can see that the area of positive baroclinic

588   conversion in the stratosphere corresponds well with the area with positive $\delta\overline{U}_z$ in HS winters,

589   so the second term should be dominant. This means that energy conversion from the zonal-mean

590   field to waves is enhanced when the vertical shear of westerlies is enhanced in the HS

591   stratosphere, which in turn enhances wave generation and accelerate zonal winds in the

592   stratosphere. These processes will therefore act as positive feedback in HS winters.

593   It should be noted that all the regressions in this study are for the case where the NAO

594   index is *positive*; if we consider the case with a negative NAO index, the polarity of the contours

595   and the direction of the arrows should all be opposite. Therefore, it is not the polarity that is the

596   problem; what needs to be clarified is the question of why the zonal wind variations associated

597   with unit changes in the NAO index are greater when solar activity is high. It is found that the

598   main mechanism to create solar cycle modulation of the NAO is the same as that associated with

599   the SAM (K18); the sensitivity of the wave-mean flow interaction is very high under high solar

600   conditions. Thus, the source should originate from dynamical properties of the basic state during

601   HS years.

602   This situation suggests that the basic state in HS winters is more unstable (especially

603   baroclinically) to changes in polar vortex than in LS winters. In fact, a larger meridional

604   temperature gradient appears from the lower to middle stratosphere in midwinter for the HS

605   winters associated with a positive change of the NAO index (Figure 3), consistent with such a

606   situation. A comparison of the stability analysis and basic state between HS and LS winters

607   should be performed in future studies.

In the present study, we focused only on the solar cycle effect of the NAO, while other factors affecting the NAO were not considered. However, previous studies showed that the solar-climate interactions tend to be strongly influenced by the equatorial Quasi-Biennial Oscillation (QBO) (e.g., Labitzke and van Loon, 1988; Kuroda, 2007; Matthes et al., 2013). In fact, Kuroda (2007) showed that the zonal wind anomalies associated with the winter-mean NAO signal tend to extend farther upward in the westerly wind phase of the QBO. Thus, it is important to examine the role of the QBO. However, it should also be noted that the sampling size tends to be almost halved if QBO effects are included. Thus, accurate analysis is possible only when more model data are available as in the study by Matthes et al., (2013). Analyses related to both the solar cycle and the QBO are left to future research.

References

Andrews, D. G., J. R. Holton, and C. B. Leovy (1987), *Middle Atmosphere Dynamics*, (p. 489), Academic Press. https://doi.org/10.1016/0019-1035(88)90078-4.

Chiodo, G. et al. (2016), The impact of a future solar minimum on climate change projection in the northern hemisphere. *Environmental Research Letters, 11,* 034015. https://doi.org/10.1088/1748-9326/11/3/034015.

Dee, D. P. *et al*. (2011), The ERA-Interim reanalysis: configuration and performance of the data assimilation system, *Q. J. R. Meteorol. Soc., 137,* 553–597, https://doi.org/10.1002/qj.828.

Eady, E. T. (1949), Long waves and cyclone waves, Tellus, 1, 33-52, https://doi.org/10.3402/tellusa.v1i3.8507.

Frame, T. H. A., and L. J. Gray (2010), The 11-yr solar cycle in ERA-40 data: an update to 2010, *J. Clim., 13,* 2213–2222, https://doi.org/10.1175/2009JCLI3150.1.

Gray, L. J. *et al.* (2010), Solar influence on climate, *Rev. Geophys., 48,* RG4001, https://doi.org/10.1029/2009RG000282.

Gray, L. J., T. J. Woollings, M. Andrews, and J. Knight, (2016), Eleven-year solar cycle signal in the NAO and Atlantic / European blocking, *Quarterly Journal of the Royal Meteorological Society, 142,* 1890-1903, https://doi.org/doi:10.1002/1j.2782.

Holton, R. J. (1975), *The Dynamic Meteorology of the Stratosphere and Mesosphere,* Meteorological Monographs, vol. 15, pp. 218, American Meteorological Society, Boston.

Hurrell, J. W., Y. Kushnir, G. Ottersen, and M. Visbeck, (edit) (2003), *The North Atlantic Oscillation*, Geophysical Monographs, (vol. 134, p. 279), American Geophysical Union, https://doi.org/10.1029/134GM01.

Kobayashi, S., et al. (2015), The JRA-55 reanalysis: General specification and basic characteristics, *J. Meteorol. Soc. Jpn, 93*, 5-48, https://doi.org/doi:10.2151/jmsj.2015-001a.

Kodera, K. (2002), Solar cycle modulation of the North Atlantic Oscillation: Implications in the spatial structure of the NAO, *Geophys. Res. Lett., 29(8)*, 1218, https://doi.org/10.1029/2001GL014557.

Kodera, K. (2003), Solar influence on the spatial structure of the NAO during the winter 1900-1999, *Geophys. Res. Lett., 30(4)*, 1175, https://doi.org/10.1029/2002GL016584.

Kodera, K., and Y. Kuroda, (2002), Dynamical response to the solar cycle, *J. Geophys. Res., 107*(D24),4749, https://doi.org/10.1002/2002JD002224.

Kuchar A., P. Sacha, J. Miksovsky, and P. Pisoft (2015), The 11-year solar cycle in current reanalyses: a (non)linear attribution study of the middle atmosphere, *Atmos. Chem. Phys., 15*, 6879-6895, https://doi.org/10.5194/acp-15-6879-2015.

Kuroda, Y. (2002), Relationship between the Polar-night Jet Oscillation and the Annular Mode, *Geophys. Res. Lett., 29 (8),* https://doi.org/10.1029/2001GL013933.

Kuroda, Y. (2007), Effect of QBO and ENSO on the solar cycle modulation of winter North Atlantic Oscillation, *J. Meteorol. Soc. Jpn, 85*, 889-898, https://doi.org/10.2141/jmsj.85.889.

Kuroda, Y. (2016), Influence of atmospheric waves on the formation and the maintenance of the subtropical jet during the northern hemisphere winter; a new method for analyzing the responses to specific forcings, *J. Geophys. Res., 121,* https://doi.org/10.1002/2015JD024592.

Kuroda, Y. (2018), On the origin of the solar cycle modulation of the southern annular mode, *J. Geophys. Res. 123,* https://doi.org/10.1002/2017JD027091.

Kuroda, Y., and K. Kodera (2002), Effect of solar activity on the polar-night jet oscillation in the northern and southern hemisphere winter, *J. Meteorol. Soc. Jpn., 80,* 973-984, https://doi.org/10.2151/jmsj.80.973.

Kuroda, Y., and K. Kodera (2005), Solar cycle modulation of the southern annular mode, *Geophys. Res. Lett., 32,* L13802, https://doi.org/10.1029/2005GL022516.

Kuroda, Y., K. Kodera, K. Yoshida, S. Yukimoto, and L. J. Gray (2022), Influence of the solar cycle on the North Atlantic Oscillation, *J. Geophys. Res., 127,* e2021JD035519, https://doi.org/10.1002/2021JD035519.

Labitzke, K., and H. van Loon (1988), Associations between the 11-year solar cycle, the QBO and the atmosphere, Part 1: The troposphere and stratosphere in the northern hemisphere in wnter, *J. Atmos. Terr. Phys.*, *50*, 197-206, https://doi.org/10.1016/0021-9169(88)90068-2.

Lu, H., A. A. Scaife, G. J. Marshall, J. Turner, and L. J. Gray (2017a), Downward wave reflection as a mechanism for the stratosphere-troposphere response to the 11-year solar cycle, *J. Clim., 30,* 2395–2414, https://doi.org/10.1175/JCLI-D-16-0400.1

Lu, H., L. J. Gray, I. P. White, and T. J. Bracegirdle (2017b), Stratospheric response to the 11-yr solar cycle: Breaking waves, internal refleclton and resonance, *J. Clim., 30,* 7169-7190, https://doi.org/10.1175/JCLI-D-17-0023.1

Matthes, K., K. Kodera, R. R. Garcia, Y. Kuroda, D. R. Marsh, and K. Labitzke (2013), The importance of time-varying forcing for QBO modulation of the atmospheric 11 year solar cycle signal, *J. Geophys. Res., 118,* 4435-4447, https://doi.org/10.1002/jgrd.50424.

Misios S. et al. (2019), Slowdown of the walker circulation at solar cycle maximum, *PNAS*, 116, 7186-7191, https://doi.org/10.1073/pnas.1815060116.

Noguchi S., and C. Kobayashi (2018), On the reproducibility of the September 2002 vortex splitting event in the Antarctic stratosphere achieved without satellite observations, *Q. J. Roy. Meteorol. Soc.*, 144, 184-194, https://doi.org/10.1002/qj.3193.

Ogi, M., K. Yamazaki, and Y. Tachibana (2003), Solar cycle modulation of the seasonal linkage of the North Atlantic Oscillation (NAO), *Geophys. Res. Lett. 30*, 2170, https://doi.org/10.1029/2003GL018545.

Thiéblemont, R., K. Matthes, N-E. Omirani, K. Kodera, and F. Hansen (2015), Solar forcing

synchronized decadal North Atlantic climate variability, *Nature Communications, 6:8268,* https://doi.org/doi:10.1038/ncomms9268.

Thompson, D.W.J. and J.M. Wallace (2000), Annular modes in the extratropical circulation. Part I: Month-to-month variability, *J. Clim., 13,* 1000–1016, https://doi.org/10.1175/1520-0442(2000)013<1000:AMITEC>2.0.CO;2